

Ruthenium(II)- bipyridyl with extended π -system: Improved thermo-stable sensitizer for efficient and long-term durable dye sensitized solar cells

M CHANDRASEKHARAM^{a,*}, G RAJKUMAR^c, CH SRINIVASA RAO^a, T SURESH^a, P Y REDDY^c and Y SOUJANYA^b

^aInorganic and Physical Chemistry Division, Indian Institute of Chemical Technology, Uppal Road, Tarnaka, Hyderabad 500 607, India

^bMolecular Modelling group, Indian Institute of Chemical Technology, Uppal Road, Tarnaka, Hyderabad 500 607, India

^cAisin Cosmos R&D Co. Ltd, Nanomaterials Laboratory, Indian Institute of Chemical Technology, Uppal Road, Tarnaka, Hyderabad 500 607, India
e-mail: chandra@iict.res.in

MS received 6 January 2011; revised 18 May 2011; accepted 19 May 2011

Abstract. A new extended thermo-stable high molar extinction coefficient bipyridyl ruthenium(II) complex “*cis*-Ru(4,4'-bis(3,5-di-*tert*-butylphenyl)-2,2'-bipyridine)(Ln)(NCS)₂ H101”, where Ln = 4,4'-dicarboxylic acid-2,2'-bipyridine; was synthesized and characterized by ¹H-NMR, FT-IR and ESI-MASS spectrometers. The H101 sensitized solar cell constructed with an active area of 0.54 cm² in combination with an ionic liquid electrolyte exhibited broader photocurrent action spectrum with solar-to-electric energy conversion efficiency (η) of 5.89 ($J_{SC} = 12.14 \text{ mA/cm}^2$, $V_{OC} = 690 \text{ V}$, fill factor = 0.699) under Air Mass (AM) 1.5 sunlight, while the reference ‘*cis*-Ru(4,4'-dinonyl-2,2'-bipyridine)(Ln)(NCS)₂’, Z907 sensitized solar cell exhibited η -value of 5.17% ($J_{SC} = 11.93 \text{ mA/cm}^2$, $V_{OC} = 650 \text{ V}$, fill factor = 0.666). TGA analysis of H101 showed extended thermal-stability and under continuous light exposure and aging at 55°C, the DSSC retained 85% of its initial η -value, while under comparable conditions Z907 sensitized solar cell retained 88%. As compared to 4,4'-dinonyl-2,2'-bipyridine in Z907, the new ancillary bipyridyl ligand ‘4,4'-bis(3,5-di-*tert*-butylphenyl)-2,2'-bipyridine’ in H101 shifts the absorption bands remarkably towards blue. The Density Functional Theory (DFT) and Time-Dependent DFT excited state calculations of the new sensitizer show that the first three HOMOs have t_{2g} character with sizeable mixing from the NCS ligands with π -bonding orbitals of 4,4'-bis(3,5-di-*tert*-butylphenyl)-2,2'-bipyridine. The LUMO is a π^* -orbital localized on the 4,4'-dicarboxylic acid-2,2'-bipyridine and higher un-occupied frontier orbitals have π^* -combinations with 4,4'-bis(3,5-di-*tert*-butylphenyl)-2,2'-bipyridine.

Keywords. Dye sensitized solar cells; extended π -system; thermo-stable; Polypyridyl Ru(II)-sensitizers.

1. Introduction

Essentially the source of all forms of energy on all planets in the solar system is coming from the Sun. The energy radiated by the Sun is about 10'000 times the currently needed energy on the Earth. Some of it being reflected back into space, a lot being absorbed by water surfaces, mountains and clouds. The irradiation variations are also moving winds and waves and evaporating water for useful precipitations for the growth of biomass and the river motions by gravity. There is a lot of potential to use all these forms of renewable

energy to cater everyday needs of the human race. Efficient trapping of sunlight and directly converting into electricity has been a challenge over the last few decades. Researchers all over the world are focussing on development of high efficient long-term durable solar cells. In this regard Silicon Solar cells have been well established as highly efficient and their uses are limited to space applications owing to the high cost involved in their manufacture. Recently among thin film photovoltaics, organic solar cells and dye sensitized solar cells gained special attention because of their high photon-to-electricity conversion efficiency, easy fabrication, low cost involved in mass production compared to the traditional photo-electrochemical cells.^{1–5} Among the various components employed

*For correspondence

in the fabrication of DSSC, sensitizer plays a key role in-terms of overall performance. Since Michael Graetzel introduced the first efficient nano-crystalline TiO_2 solar cell sensitized with *cis*-bis(thiocyanato) *bis* (2,2'-bipyridyl-4,4'-dicarboxylato) ruthenium(II) *bis*(tetrabutylammonium) (**N719**), a variety of ruthenium(II) polypyridyl complexes, porphyrins, phthalocyanines and metal free organic sensitizers have been developed.^{6–17} Over the last two decades, there have been considerable interest to improve the overall solar-to-electrical energy conversion efficiency (η) of the DSSC devices by modifying the structure of sensitizers and varying the other components of the device. For instance, one of the bipyridyl ligand of **N719** was substituted with alkoxy styryl, triethyleneoxy (ion coordinating) styryl, *tert*-butoxy styryl, etc. groups with the concept of increase in the π -conjugation extension for high molar extinction coefficient dyes or optimizing the DSSC fabrication conditions with suitable electrolyte and favourable texture of the nanocrystalline TiO_2 electrodes.^{16,18–20} But long-term device durability is found to be one of the key limitations of DSSC device for outdoor application. The leakage of liquid electrolyte, desorption of loosely anchored dye molecules, and photo-degradation of the dye anchored on TiO_2 as well as corrosion of the Pt counter electrode by the triiodide/iodide couple have been suggested as the factors responsible for limiting the long-term performance of DSSC. To overcome this, new counter-electrode materials,^{21–23} alternative redox couples^{24–26} such as solid state or quasi-solid-state electrolytes have been thoroughly studied. In this regard **Z907** and **K77** dyes showed considerable long term durability with moderate conversion efficiencies. However, achievement of high device conversion efficiency along with long-term durability remains a major challenging task.^{13,27–36} Substituted bipyridines recently attracted special attention for their importance in biological applications as Zn^{2+} specific fluorescent molecular probes.^{37–39} We developed ruthenium(II) bipyridyl complexes *cis*-Ru(4,4'-*bis*(3,5-di-*tert*-butylstyryl)-2,2'-bipyridine)(Ln)(NCS)₂ '**HRD1**' and *cis*-Ru(4,4'-*bis*(2,4,6-trimethylstyryl)-2,2'-bipyridine)(Ln)(NCS)₂ '**HRD2**' where Ln = 4,4'-dicarboxylic acid-2,2'-bipyridine, which have shown good conversion efficiencies along with device durability comparable with **K77** sensitized solar cells.⁴⁰ The ruthenium (II) complexes, **H112**,⁴¹ **PTZ1**,⁴² **mLBD1** and **mLBD2**⁴³ developed in our laboratory with π -conjugation extension also showed moderate efficiency in DSSC device. Recently ruthenium(II) complexes with the alkyl substituted aryl moieties directly connected to

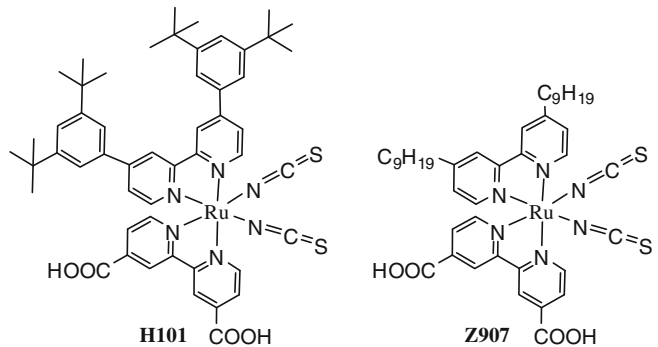


Figure 1. Structure of **H101**.

bipyridines as ancillary ligand have shown substantial improvement in the solar-to-electrical energy conversion efficiency^{16,44,45} and it seems to be reasonable to explore further these non-vinylogous structures for achieving better overall performance in photovoltaic devices. In this regard, a new ancillary bipyridyl ligand 4,4'-*bis*(3,5-di-*tert*-butylphenyl)-2,2'-bipyridine (**L1**) was designed (figure 1) and synthesised by coupling the corresponding 3,5-di-*tert*-butylphenylboronic acid with 4,4'-dibromo-2,2'-bipyridine under palladium catalysed Suzuki conditions.^{46,47} This ligand was successfully employed to synthesize the corresponding polypyridyl ruthenium(II) complex '*cis*-Ru(**L1**) (4,4'-dicarboxylic acid-2,2'-bipyridine)(NCS)₂ **H101**'. In this paper, we presented the synthesis and the photovoltaic characteristics of **H101** sensitized solar cell fabricated with an active area of 0.54 cm² dye sensitized TiO_2 electrodes in conjunction with ionic liquid electrolyte. The photovoltaic characteristics of the sensitizer were compared with reference **Z907** cell fabricated and measured under identical conditions.

2. Experimental

2.1 General

1-bromo-3, 5- di-*tert*-butyl benzene, *n*-BuLi, Pd(PPh₃)₄, NH₄NCS, 1,2-dimethyl-3-*n*-propylimidazolium iodide (DMPII), 4-*tert*-butylpyridine (TBP), hexachloroplatinic acid, tetrabutylammoniumhydroxide (TBA) were purchased from Sigma-Aldrich. 4,4'-dibromo 2,2'-bipyridine was procured from Heterocycles and Catalysts, Gundeldingerstrasse 174, CH-4053 Basel, Switzerland. Sephadex LH-20 was procured from GE Healthcare Bio-Sciences AB, SE-75184, Uppsala. Dichloro (*p*-cymene) ruthenium (II) dimer and 2,2'-bipyridine-4,4'-dicarboxylic acid were prepared in accordance to the reported procedures.^{48,49} All solvents

and reagents, unless otherwise stated, were of Laboratory Reagent Grade and used as received. Bruker 300 Avance ^1H NMR spectrometer, Shimadzu LCMS-2010EV model with ESI probe, Shimadzu UV-Vis spectrometer (Model: UV-1700) and Fluorolog 3, J.Y. Horiba Fluorescence spectrometers were employed to characterize 4,4'-*bis*(3,5-di-*tert*-butylphenyl)-2,2'-bipyridine, and the new polypyridyl ruthenium(II) complex (**H101**). 4, 4'-dinonyl-2,2'-bipyridine (**L2**) was procured from Sigma-Aldrich.

2.1a Synthesis of 3, 5-di-*tert*-butylphenylboronic acid: To a stirring cooled (-78°C) solution of 1-bromo-3, 5-di-*tert*-butyl benzene (500 mg, 1.858 mmol) in dry tetrahydrofuran, *n*-BuLi (1.394 ml, 1.6 M in hexane) was added drop-wise under nitrogen atmosphere. After stirring continued for 1 h, triisopropyl borate (0.642 ml, 2.787 mmol) was added at the same temperature. The reaction mixture was further stirred for 2 h, and quenched with water followed by 6M HCl solution drop-wise until pH dropped below 7.0. The resulting mixture was poured into water and then extracted with dichloromethane. The combined organic layers were dried over anhydrous sodium sulphate and after evaporation of dichloromethane under a reduced pressure, the resulting solid was purified by column chromatography on silica gel with dichloromethane/methanol (9/1) as eluent to afford 3,5-di-*tert*-butylphenylboronic acid (239 mg, 55% yield).

$^1\text{H-NMR}$ ($\delta\text{H}/\text{ppm}$ in CDCl_3): 7.45 (s, 1H), 7.11 (s, 2H), 2.00 (s, 2H), 1.40 (s, 18H). Chemical formula $\text{C}_{14}\text{H}_{23}\text{BO}_2$, ESIMS: Calcd for $(\text{M}+\text{H})^+$: 234, found: 234.

2.1b Synthesis of 4,4'-*bis*(3,5-di-*tert*-butylphenyl)-2,2'-bipyridine (L1**):** In a 25 ml one-necked round bottom flask equipped with a condenser were placed corresponding boronic acid (1.528 mmol), barium hydroxide octa-hydrate (1.5 g, 4.77 mmol) and palladium tetrakis triphenyl phosphine (146 mg, 0.127 mmol). The reaction flask was evacuated and filled with nitrogen gas, then 1, 4-dioxane/water (v/v, 3:1, 8 ml) and 4,4-dibromo-2,2'-bipyridine (200 mg, 0.636 mmol) were added. The reaction mixture was refluxed for 24 h under nitrogen gas and cooled to room temperature. The dioxane was removed and the contents were poured into dichloromethane, the precipitate formed was removed by filtration through filter paper and the organic layer was washed with 1.0 m NaOH aqueous solution, and dried over sodium sulphate. After evaporation of dichloromethane under

a reduced pressure, the resulting residue was diluted with a small quantity of methanol. The precipitate formed was immediately filtrated, dried and purified by column chromatography on silica gel with dichloromethane/methanol (9/1) as eluent to afford the corresponding ligand (447 mg, 55% yield).

$^1\text{H-NMR}$ (CDCl_3) 1.35 (s, 9H), 6.82 (d, 1H), 6.97 (s, 2H), 7.30 (s, 1H), 8.07 (s, 1H), 8.50 (d, 1H); Chemical formula $\text{C}_{38}\text{H}_{48}\text{N}_2$, ESIMS: Calcd for $(\text{M}+\text{H})^+$: 532, found: 532.

2.1c Synthesis of H101: Compound 4,4'-*bis*(3,5-di-*tert*-butylphenyl) - 2,2'- bipyridine (0.902 mmol) and dichloro (*p*-cymene) ruthenium(II) dimer (276 mg, 0.451 mmol) in DMF were heated at 60°C for a period of 4 h under nitrogen in the dark. Subsequently, 4,4'-dicarboxylic acid-2, 2'-bipyridine (220 mg, 0.902 mmol) was added and the reaction mixture was heated to 140°C for another 4 h. To the resulting dark green solution was added solid NH_4NCS (2.060 g, 22.064 mmol) and the reaction mixture was further heated for 4 hours at 140°C . After evaporation of DMF, water (250 ml) was added to get precipitate. The purple solid was filtered off, washed with water and ether, and dried under vacuum. The crude compound was dissolved in methanol and dichloromethane and purified by column chromatography on Sephadex LH-20 with methanol/dichloromethane (3/2) as eluent to afford ruthenium complex (582 mg, 65% yield).

$^1\text{HNMR}$ ($\text{CDCl}_3 + \text{CD}_3\text{OD}$): 1.31 (s, 18H), 1.40 (s, 18H), 6.52 (d, 1H), 6.89 (s, 2H), 7.00 (d, 1H), 7.15 (s, 2H), 7.20 (d, 1H), 7.36 (s, 1H), 7.50 (s, 1H), 7.59 (s, 1H), 7.73 (d, 1H), 7.88 (s, 1H), 7.98 (d, 1H), 8.20 (d, 1H), 8.80 (s, 1H), 8.91 (s, 1H), 9.20 (d, 1H), 9.72 (d, 1H).

2.2 Fabrication and photocurrent-voltage measurements of the nanocrystalline TiO_2 solar cells

The test cells were fabricated using 0.54 cm^2 active area TiO_2 electrodes in combination with I^-/I_3^- redox couple electrolyte. Initially the fluorine-doped SnO_2 (FTO) conducting glass plates (Nippon Sheet Glass, 4 mm thick, $8\ \Omega/\text{sq}$) were cleaned with a detergent solution and then rinsed with water and ethanol to remove organics or any other contaminants, the dried glass plates were then treated in a UV-O₃ system for 20 minutes. To facilitate a good mechanical contact between the nanocrystalline TiO_2 and the conducting FTO matrix, the cleaned plates were treated with a 40 mM TiCl_4 aqueous solution and then heated at 70°C for 30 minutes. Over the glass plate, 9 μm thickness layer of 18 nm

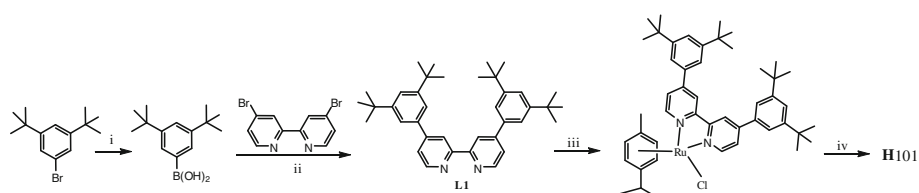
TiO_2 particles (D18T) as transparent layer and then a $4.8\ \mu\text{m}$ thickness layer of 400 nm anatase TiO_2 particles (CCIC, HPW-400) as scattering layer were successively laid one over the other. The electrodes coated with the TiO_2 pastes were heated gradually under an air flow for 5 minutes each at 325°C and 375°C and for 15 minutes each at 450°C and 500°C . The TiO_2 electrodes were then allowed to cool and when the temperature attained around 100°C , immersed in dye solutions of ethanol and remained soaked for 16 hours under dark. After taking out from the dye solutions, the electrodes were rinsed with ethanol to remove the un-adsorbed dye molecules and then dried under nitrogen gas. The counter electrodes were prepared by treatment of FTO glass plates (TEC 15, 2.2 mm thickness, Libbey-Owens-Ford Industries) with TiCl_4 and further with a drop of H_2PtCl_6 solution (2 mg of Pt in 1 mL of ethanol) and heated at 430°C for 15 minutes. The dye sensitized TiO_2 electrode and Pt counter electrode were assembled into a sealed sandwich type cell by heating with a hot-melt surlyn film (Surlyn 1702, $25\ \mu\text{m}$ thickness, Du-Pont) as a spacer in-between the electrodes. The ionic liquid electrolyte was filled through the predrilled hole present on the counter electrode using vacuum filling technique, the hole was sealed with a Surlyn disk and a thin glass to avoid leakage of the electrolyte. The photo current-voltage measurements of the DSSC devices fabricated were executed under the irradiation source of 450 W Xenon light (Osram XBO 450, U.S.A.), whose power was equivalent to AM 1.5 solar simulator. Prior to these measurements, the xenon light was calibrated by using a Tempax 113 solar filter (Schott) and the output power of the solar simulator was calibrated by using a reference Si photodiode equipped with a coloured matched IR-cut-off filter (KG-3, Schott) to reduce the mismatch in the region of 350–750 nm between the simulated light and AM 1.5 to <2%. The measurement delay time of photo I – V characteristics of DSSCs was fixed at 40 ms. The incident light from a 300 W xenon lamp (ILC Technology, U.S.A.), which was focused through

a Gemini-180 double monochromator (Jobin Yvon Ltd.), was employed to plot incident photon-to-current conversion efficiency as a function of excitation wavelength.

3. Results and discussion

3.1 Synthesis

The new polypyridyl ruthenium(II) complex, **H101** (figure 1) was synthesized in accordance to the sequence of steps illustrated in Scheme 1. 1-bromo-3,5-di-*tert*-butylbenzene was subjected to bromine-lithium exchange reaction using *n*-butyllithium in the presence of tri-isopropyl borate to give 3,5-di-*tert*-butylphenylboronic acid, which was reacted with 4,4'-dibromo-2,2'-bipyridine under $\text{Pd}(\text{PPh}_3)_4\text{Cl}_2$ catalysed Suzuki conditions to afford ‘4,4'-bis(3,5-di-*tert*-butylphenyl)-2,2'-bipyridine’ (**L1**). The reaction of $[\text{RuCl}_2\text{p-cymene}]_2$ and **L1** in DMF followed by addition of 2,2'-bipyridine-4,4'-dicarboxylic acid and excess ammonium thiocyanate finally afforded the ruthenium complex. The crude dried compound was purified on Sephadex LH20 column chromatography using methanol/dichloromethane (1/1 V/V) mixture as eluent. The bipyridine ligand **L1** and the ruthenium(II) complex, **H101** have been fully characterised with ^1H NMR, FT-IR and ESI-MASS Spectroscopies (figures S1 to S5 in the Supporting Information). The FTIR spectra (figure S7) of **H101** show the bands at around $1610\ \text{cm}^{-1}$ and $1383\ \text{cm}^{-1}$ for the asymmetric and symmetric stretching modes of the carboxylate groups. The stretching bands at around $2100\ \text{cm}^{-1}$ correspond to NCS groups indicating that NCS coordinated to the ruthenium center through the N-atom. The stretching bands at around 2961 to $2865\ \text{cm}^{-1}$ correspond to the aryl-*tert*-butyl groups, while the absorption bands at 1540 and $1463\ \text{cm}^{-1}$ are ascribed to bipyridyl modes. The larger broad stretching band



Scheme 1. Synthesis of **H101** sensitizer. i) Tri-isopropylborate, *n*-BuLi, THF, at -78°C , 2M HCl; ii) $\text{Ba}(\text{OH})_2\cdot 8\text{H}_2\text{O}$, $\text{Pd}(\text{PPh}_3)_4$, Dioxane: H_2O , reflux for 24 h; iii) $\text{Ru}\text{-p-cymene}$ complex, DMF, reflux for 12 h; iv) 2,2'-bipyridine-4,4'-dicarboxylic acid, NH_4NCS , DMF, reflux for 12 h.

centered at 3397 cm^{-1} is due to the moisture adsorbed by the dye. The reference ruthenium(II) complex, *cis*-Ru(4,4'-dinonyl-2,2'-bipyridine)(4,4'-dicarboxylic acid-2,2'-bipyridine))(NCS)₂ (**Z907**) was synthesized in accordance to the reported procedure.¹⁸

3.2 Electronic absorption, emission and electrochemical properties of the dyes

Equi-molar dye solutions of **H101** and **Z907** were prepared in ethanol and their comparative electronic absorption spectra recorded as a function of wavelength is shown in figure 2. The molar absorptions were recorded at μM dye concentrations, which are highly dilute as compared to those employed for staining the TiO_2 electrodes. **H101** shows well-defined two intense metal-to-ligand charge transfer transition (MLCT) absorption bands one in short wavelength region and the other one in long wavelength region. The molar extinction coefficient (ϵ) of low-energy absorption band of **H101** is $15000\text{ M}^{-1}\text{ cm}^{-1}$ at 531 nm , while the reference sensitizer, **Z907**, showed ϵ -value of $10,800\text{ M}^{-1}\text{ cm}^{-1}$ at 540 nm . Although, the MLCT absorption bands are blue shifted significantly in the high-energy region, as compared to those of **Z907**, the sensitizer showed relatively $1/3$ improvement in molar absorptivity across the spectral range of $400\text{--}750\text{ nm}$. Besides the molar extinction coefficient, the light-harvesting ability of DSSCs are also influenced by the optical absorptivity of sensitizer anchored on mesoporous TiO_2 electrodes, which indirectly depend on molecular geometry and size. The absorption

measurements of the dye coated on TiO_2 electrodes were carried out by staining $7.0\text{ }\mu\text{m}$ thick TiO_2 (18 NRT layered) films in the 0.3 mM dye solutions for a period of 16 h under dark. The absorption spectra of **H101** dye coated TiO_2 film is compared with that of **Z907**. Figure S8 (Supporting Information) indicates that the dye molecules are anchored on TiO_2 surface. The film absorbance ratio of **H101** sensitizer (0.936) calculated by dividing the absorption maxima of **H101** (0.9299) with the absorption maxima of **Z907** sensitizer (0.9935) is relatively lower and indicates lower packing density of **H101** on TiO_2 surface. The substitution of *4, 4'-bis(3,5-di-*tert*-butylphenyl)* on the ancillary bipyridine in **H101** increases the diagonal size of the dye molecule as predicted resulting in lower packing density of the dye on the TiO_2 surface.⁵⁰

In DSSCs, favourite energy offset between dye and titania is an essential requirement for achieving high-efficiency, in which the sensitizer's immediate charge generation yield from the excited state has a direct influence on the device operation. The redox potentials of **H101** were scrutinized with cyclic voltammetry using tetra-butyl ammonium perchlorate (0.1 M in acetonitrile) as an electrolyte and ferrocene as an internal standard at 0.42 V vs SCE . Figure S9 (supporting information) shows the cyclic voltammogram of **H101** measured in DMF solvent. The oxidation potential obtained for **H101** sensitizer was 0.918 V , while the reduction potential was -0.810 V vs SCE. The more positive potential of this sensitizer, relative to I^-/I_3^- redox couple in the electrolyte, provide a large thermodynamic driving force for the regeneration of the dye by iodide. Based on absorption and emission spectra recorded in ethanol by exciting the complex with its corresponding low-energy absorbance maximum, the excitation transition energy (E_{0-0}) of **H101** was estimated to be 1.85 eV and the standard potential ($\phi^0(\text{S}/\text{S}^*)$), calculated from the relation of $[\phi^0(\text{S} + / \text{S}) = \phi^0(\text{S} + / \text{S}^*) - E_0 - 0]$, was -0.9341 V vs SCE. So, $\phi^0(\text{S}/\text{S}^*)$ value of the **H101** dye is more negative (or higher in energy) than the conduction band edge of TiO_2 , providing a thermodynamic driving force to inject electron from the dye to TiO_2 .

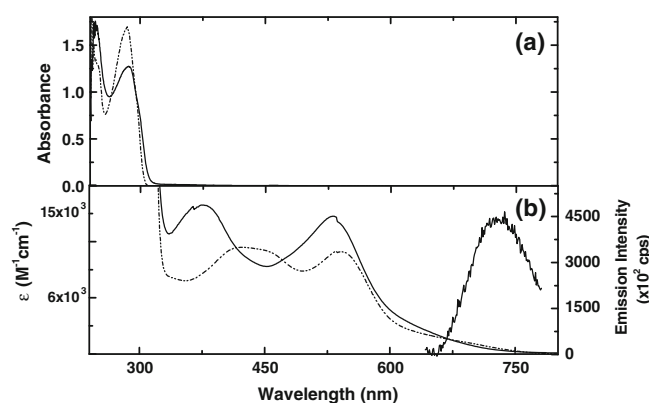


Figure 2. (a) Equi-molar absorption spectra of (—) *4,4'-bis(3,5-di-*tert*-butylphenyl)-2,2'-bipyridine* and (---) *4,4'-dinonyl-2,2'-bipyridine* in DMF. (b) Electronic absorption spectra of (—) **H101** and (---) **Z907** sensitizers in DMF medium.

3.3 Computational studies

To understand the increase in molar extinction coefficient augment with extension of π -conjugation through *4,4'-bis(3,5-di-*tert*-butylphenyl)-2,2'-bipyridine* (**L1**) in **H101**, DFT geometry optimization and Time Dependent DFT excited state calculations for electronic

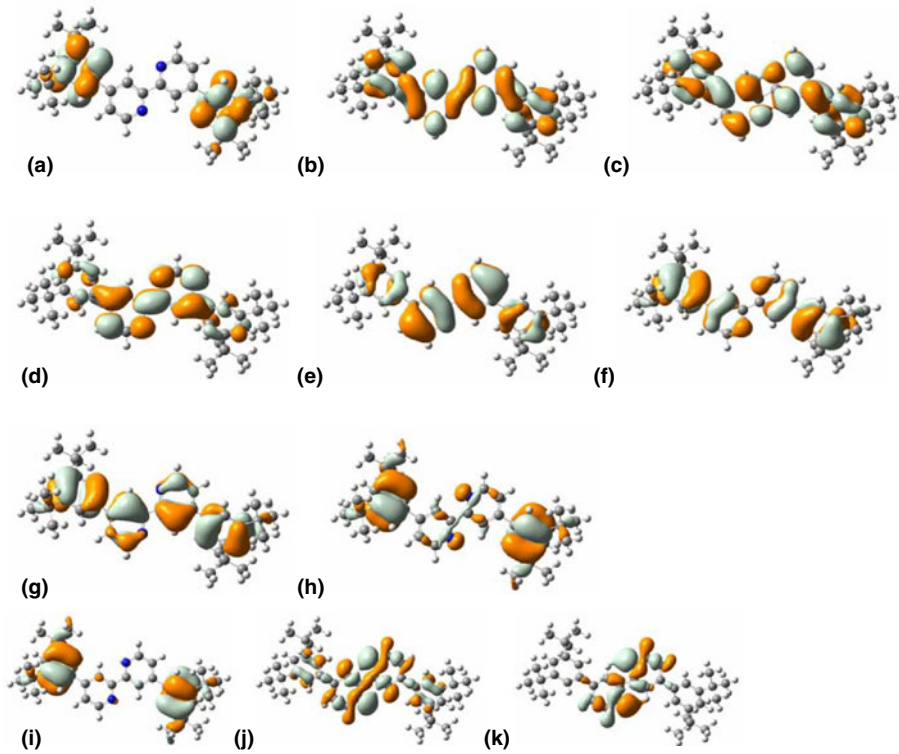


Figure 3. Transition involved molecular orbitals of ancillary ligand **L1** of **H101**: (a) LUMO+3; (b) LUMO+2; (c) LUMO+1; (d) LUMO; (e) HOMO; (f) HOMO-1; (g) HOMO-2; (h) HOMO-3; (i) HOMO-4; (j) HOMO-5; (k) HOMO-6.

ground states of **L1**, 4,4'-dinonyl-2,2'-bipyridine (**L2**), protonated ruthenium(II) complexes (**H101** and **Z907**) were performed by using mPW(mPWx+PW91c) parameterization method. The combination of the Perdew–Wang 1991 exchange functional and modified by Adamo and Barone (mPWx) with the Perdew and Wang's 1991 gradient corrected correlation functional (PW91c) being developed along with mixed basis, LANL2DZ for ruthenium and 6-31G(d) basis for other atoms have been used in Gaussian 03.⁵¹ The transition involved frontier molecular orbitals (HOMO-6 to HOMO and LUMO to LUMO+3) of **L1** are shown in figure 3, while those of **L2** (HOMO-4 to HOMO and LUMO to LUMO+3) are shown in figure S10 in the Supporting Information. The HOMO-6 and HOMO-7 orbitals of **L1** resemble HOMO-1 and HOMO-2 orbitals of **L2** and their energy levels shown in figure 5 are found to be close to one another. The π -orbitals corresponding to HOMO-1 to HOMO-3 of **L1** are delocalized among the phenyl units (π -system) and pyridines, while LUMO to LUMO+3 orbitals have more π^* -orbital delocalization and the corresponding energy levels are depressed as compared to those of **L2**. The electronic absorption spectra recorded at equimolar concentration (figure 2a) showed lower molar

absorptivity along with bathochromic shift by 6 nm for **L1** relative to **L2**. The TD-DFT excitation calculations of these ancillary ligands showed lower oscillation strength for **L1** with bathochromic shift by around 10 nm (table S1, Supporting Information) which indicate that the predictions of photophysical properties are close to the experimental observations.

Ancillary ligands with various extended π -conjugation systems in the ruthenium(II) complexes are known to improve ε -value along with significant bathochromic shift. To predict the influence of 3,5-di-*tert*-butyl phenyl as π -conjugation extension, the occupied and unoccupied frontier orbitals of **H101** are shown in figure 4, while those of **Z907** are compared (figure S11, Supporting Information). The first three occupied (HOMO to HOMO-2) orbitals of **H101** exhibit ruthenium t_{2g} character, a sizeable contribution resulting from the mixing of thiocyanate ligand with π -bonding orbitals of 4,4'-*bis*(3,5-di-*tert*-butylphenyl)-2,2'-bipyridine and 4,4'-dicarboxylic acid-2,2'-bipyridine. The delocalized π -orbitals in HOMO to HOMO-2 orbitals of 4,4'-*bis*(3,5-di-*tert*-butylphenyl)-2,2'-bipyridine favours size mixing with ruthenium(II)-NCS in **H101** as compared to those in 4,4'-dinonyl-2,2'-bipyridine of **Z907**, which

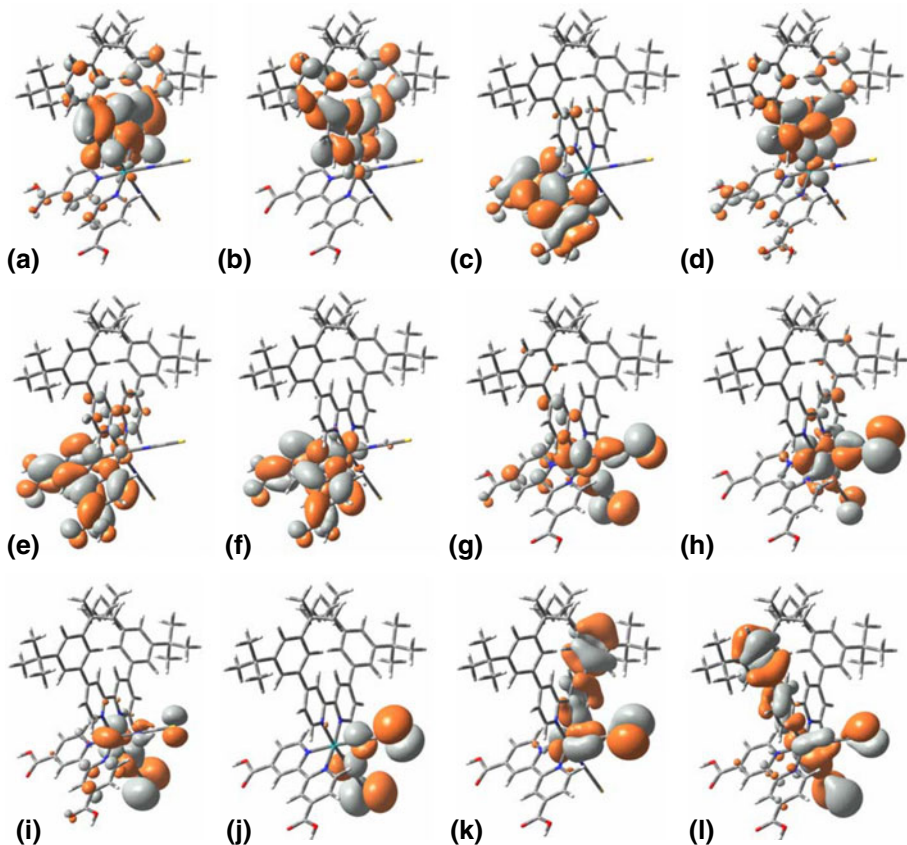


Figure 4. Frontier molecular orbitals of **H101**: (a) LUMO+5; (b) LUMO+4; (c) LUMO+3; (d) LUMO+2; (e) LUMO+1; (f) LUMO; (g) HOMO; (h) HOMO-1; (i) HOMO-2; (j) HOMO-3; (k) HOMO-4; (l) HOMO-5.

contributes to lift their energy levels. For **Z907** and **H101**, the HOMO-3 orbitals are non-bonding combination localized on the NCS ligands. But relative to **Z907** sensitizer, the increased molar extinction coefficient of **H101** could be attributed to the lifted HOMO energy level. The HOMO-4 and HOMO-5 of **H101** are combinations of two π -bonding orbitals of **L1** with significant size mixing from NCS ligands and ruthenium centre, lift their energy levels. In case of the LUMO orbitals, it is noted that there is no obvious variation because of the sole distribution moved towards 4,4'-dicarboxylic acid-2,2'-bipridine and assuming similar molecular orbital geometry when adsorbed on TiO_2 surface, the close position of the LUMO to the anchoring moieties will enhance overlap with the 3d orbitals of TiO_2 leading to facile electron injection. In case of higher unoccupied molecular orbitals of ancillary bipyridyl ligand, **L1**, the π^* -orbitals move from π -system to bipyridine moieties and these transfer in **H101** sensitizer significantly depress the LUMO+4 and LUMO+5 orbitals and a moderate extending in case of LUMO+1 orbital relative to those of **Z907**.

3.4 Photovoltaic performance of DSSCs based on the dyes

To evaluate the performance of the new ruthenium(II) bipyridyl sensitizer, we employed a high-quality double-layer titania film ($9.0 + 4.8 \mu\text{m}$) and the most compatible electrolyte (**Z580**, containing 0.2 M I_2 , 0.5 M guanidinium thiocyanate and 0.5 M *N*-methylbenzimidazole in a mixture of 1-propyl-3-methylimidazolium iodide/1-ethyl-3-methyl imidazoliumtetracyanoborate (65/35, v/v)) to construct the test cells. Iodide-based ionic liquids are more viscous than conventional organic solvents. To reduce the viscosity of these electrolytes to some extent a binary ionic liquid electrolytes prepared by mixing iodide based ionic liquids (which can act both as a solvent and an iodide source) with low viscosity ionic liquids (having weakly coordinating anion based ionic liquids). The components in **Z580** electrolyte meet the above requirements and apart from that Guanidinium thiocyanate in the redox electrolyte increases V_{OC} by slowing recombination and also by inducing a downward

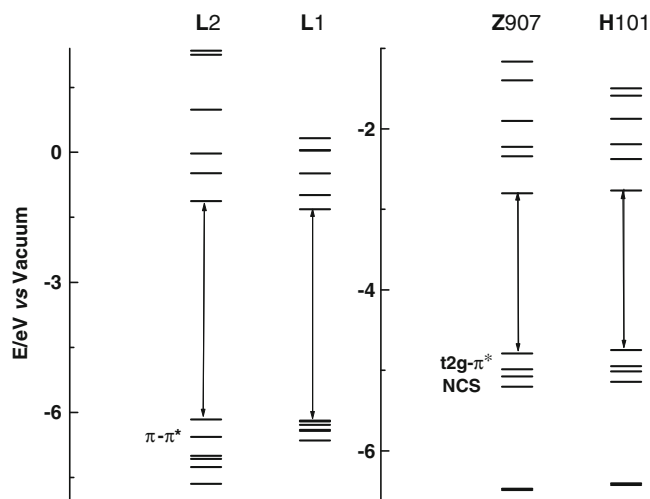


Figure 5. Energy diagram of occupied (HOMO to HOMO-5) and unoccupied (LUMO to LUMO+5) frontier orbitals of 4,4'-bis(3,5-di-*tert*-butylphenyl)-2,2'-bipyridine (**L1**); 4,4'-dinonyl-2,2'-bipyridine (**L2**), **Z907** and **H101** sensitizers.

shift of the TiO_2 conduction band edge.⁵² The incident photon-to-current conversion efficiency (IPCE) of **H101** sensitized DSSC plotted as a function of excitation wavelength (figure 6) showed broad plateau IPCE spectrum with IPCE exceeding 92.5%. Considering the light absorption and scattering loss by the conducting glass, the absorbed photon-to-collected electron conversion efficiencies (APCE) are close to unity over a broad spectral range, suggesting a very high charge collection yield. To see the effect of light-harvesting enhancement due to increased π -conjugation extension, the photocurrent action spectrum of **H101** was compared

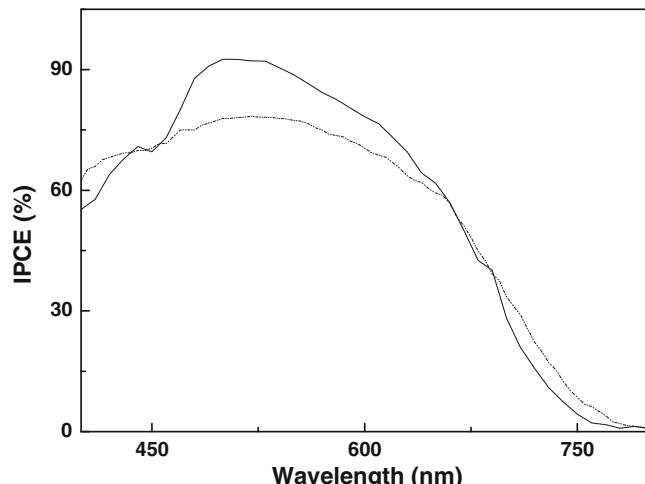


Figure 6. Photocurrent action spectra of devices of (—) **H101** and (···) **Z907** fabricated from 0.54 cm^2 active area TiO_2 electrodes sensitized in dye solutions of ethanol.

with that of **Z907** sensitized DSSC fabricated and evaluated under identical conditions. A lower IPCE value reaching 78.6% with broad plateau relatively red shifted as compared to **H101** sensitizer was observed for **Z907**. Owing to the lower packing density of **H101** over TiO_2 surface, the **H101** sensitized cell is expected to show a lower performance when compared to that of **Z907** sensitized solar cell but the higher J_{SC} of **H101** could be probably favoured by more localized electron cloud over the 4,4'-dicarboxylic-2,2'-bipyridine in LUMO of **H101** as compared to those in **Z907** sensitizer. Figure 7 shows a typical photocurrent density–voltage curve of **H101** sensitized solar cell measured under AM 1.5 sun-light illumination. The short-circuit photocurrent density (J_{SC}), open-circuit voltage (V_{OC}), and fill factor (ff) are 12.14 mA cm^{-2} , 690 mV and 0.699 , respectively, yielding an overall energy conversion efficiency (η) of 5.89%, while the test device fabricated under identical conditions with **Z907** dye gave J_{SC} of 11.93 mA cm^{-2} , V_{OC} of 650 mV , and ff of 0.666 yielding an overall energy conversion efficiency of 5.17%.

One of the desirable parameters to retain the initial photovoltaic performance of the DSSC is the high thermal stability of the ruthenium(II) sensitizer.¹⁸ To see initially the influence of *bis*(3,5-di-*tert*-butylphenyl) substitution on the thermal stability of the new ruthenium(II) sensitizer, **H101**, TGA analysis was performed using a TGA/SDTA 851^e thermal system (Mettler

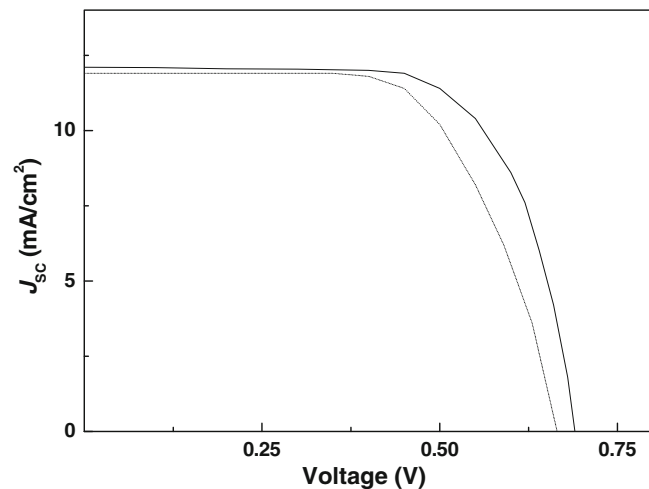


Figure 7. J – V characteristics of (—) **H101** and (···) **Z907** cells (fabricated from 0.54 cm^2 active area TiO_2 electrodes), measured under an irradiance of 100 mW cm^{-2} AM1.5G sun light. Double layer films ($9.0 + 4.8 \mu\text{m}$). The electrolyte composition: 0.2 M I_2 , $0.5 \text{ M guanidinium thiocyanate}$ and $0.5 \text{ M N-methylbenzimidazolium iodide/1-ethyl-3-methylimidazoliumtetracyanoborate}$ (65/35, v/v).

Toledo, Switzerland) at heating rate of 10°C/min in the temperature range of 25–600°C under N₂ atmosphere (flow rate of 30 ml/min). Film samples ranging from 8 to 10 mg were placed in the sample pan and heated, while weight loss and temperature difference were recorded as a function of temperature. The thermo-gram thus obtained was compared with that of Z907. Figure S12(a) in supplementary information shows the derivative of per cent of conversion with respect to temperature, wherein both the thermo-grams of H101 and Z907 initially follow similar trend and relatively extended thermal stability by another 30°C was observed for H101. In order to investigate further, the factors contributing for the increased thermal stability of the ruthenium(II) complex, the TGA analysis of ancillary ligands L1 and L2 are shown in figure S12(b) (supplementary information). The thermo-gram of L2 shows a transition at 420°C, while that of L1 shows at around 470°C yielding an increase in thermal stability by 50°C, which could be attributed to the conjugation of aromatic phenyl units against nonyl moieties on bipyridine. During the metal complex formation, these aromatic alkyl-substituted phenyl units have no effect on chelating bonds of ruthenium-bipyridine and thereby the substitution of 4,4'-bis(3,5-di-*tert*-butylphenyl)-2,2'-bipyridine in place of 4,4'-dinonyl-2,2'-bipyridine further stabilizes. This extended thermal stability is expected to improve the long term durability of photovoltaic performance of the sensitizer in DSSC.

The photovoltaic characteristics of H101 sensitized solar cell were measured at various temperatures by annealing the solar device in the pre-heated oven set

at the desired temperature and were plotted as a function of temperature. Figure 8 shows a slight change in both V_{OC} and fill factor across the temperature range of 30 to 80°C, while a gradual increase in photo-current density, J_{SC} was observed with increasing temperature of the device, which ultimately translated to gradual increase in the overall energy conversion efficiency. The photostability studies for these ruthenium(II) bipyridyl complexes were performed under a solar simulator at 100 mWcm² intensity. The H101 sensitized solar cell covered with an ultraviolet absorbing polymer film showed a nominal decrease in its initial η -value after 1,000 h of light-soaking at 55°C. The aging tests have been performed at 55°C for 1000 h (figure 9), the power conversion efficiency of H101 sensitized solar cell was sustained even under heating, maintaining 85% of its initial value after this time period, while Z907 device retained 88% of its initial performance, despite the fact that the sustainability of the cell initial efficiency varies based on the type of electrolyte employed in the fabrication of DSSC. The retainability of initial efficiency for H101 sensitizer is slightly lower as compared to that of Z907. To understand this, a series of desorption studies of H101 and Z907 sensitized TiO₂ films in KOH-solutions were carried out separately to evaluate the desorption pattern of these dyes from TiO₂ films. Though the results showed that desorption of H101 from TiO₂ is quantitatively little more compared to that of Z907, the retainability of H101 sensitized solar cell is comparable with that of Z907 sensitizer and the relatively higher efficiency observed after complete aging of 1000 h at

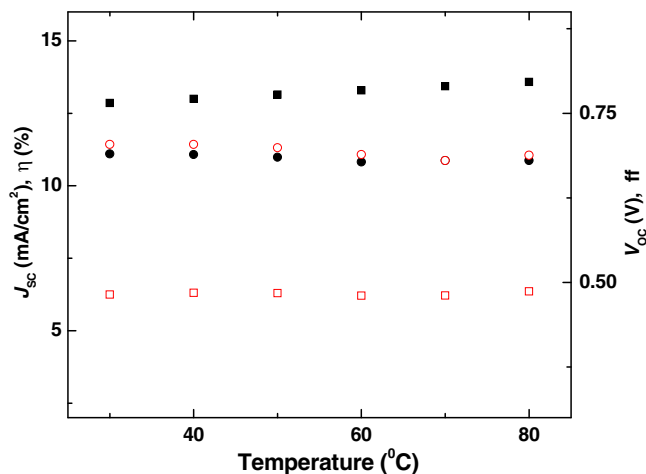


Figure 8. Detail of device parameter variations with temperature; (■) Short-circuit photocurrent density; (□) energy conversion efficiency; (○) open current voltage; (●) fill factor.

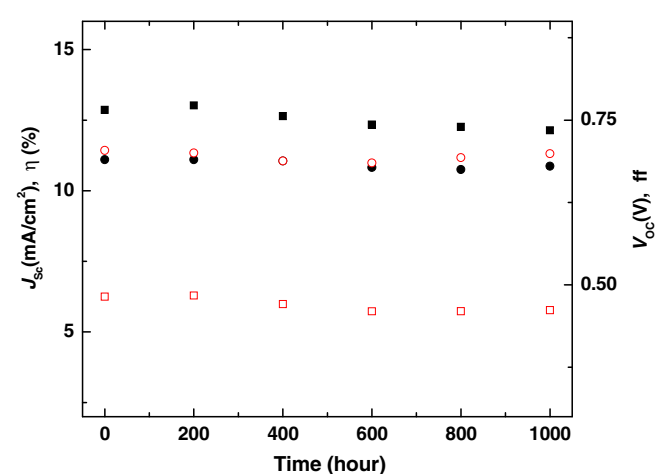


Figure 9. Details of device parameter variations for cells during accelerated aging at 50°C; (■) Short-circuit photocurrent density; (□) energy conversion efficiency; (○) open current voltage; (●) fill factor.

55°C is presumed to be resulting from the substitution of 4,4'-*bis*(3,5-di-*tert*-butylphenyl)-2,2'-bipyridine against 4,4'-dinonyl-2,2'-bipyridine in Z907 sensitizer. The main disadvantage of the π -extension (C=C double bond) in ruthenium(II)-bipyridyl sensitizers is the slight catalysis of the electron/electrolyte recombination, which could be resulting through the vinylene spacers. The new ruthenium(II)-bipyridyl sensitizer, H101 is designed with exclusion of ethenyl spacers and the long-term device durability studies of the device indicate that the four *tert*-butyl groups on phenyl units of the ancillary bipyridyl ligand gives similar effect in terms of compatibility with ionic liquid electrolyte as observed with two *n*-nonyl groups of Z907.

4. Conclusions

To summarise, a high molar extinction coefficient ruthenium(II) sensitizer, exhibiting 5.89% power conversion efficiency for 0.54 cm² active area DSSC under AM 1.5 G conditions, has been synthesized using 4,4'-*bis*(3,5-di-*tert*-butylphenyl)-2,2'-bipyridine as π -conjugated ancillary ligand. The TGA analysis of H101 showed relatively extended thermal stability, when compared to that of reference Z907 sensitizer. The sensitizer showed better incident photon-to-collected electron conversion efficiency and higher overall photovoltaic performance before and after completion of aging studies.

Supplementary information

The electronic supplementary information can be seen in www.ias.ac.in/chemsci.

Acknowledgements

Ch S R thanks Indian Institute of Chemical Technology-Aisin Cosmos (IICT-AIC) collaborative project for a fellowship. TS thanks Council of Scientific and Industrial Research (CSIR), New Delhi for senior research fellowship. MC thanks Department of Science and Technology (DST) New Delhi for the grant of the project entitled 'Advancing the efficiency and production potential of Excitonic Solar Cells (APEX)' under UK-DST consortium.

References

1. Benkstein K D, Kopidakis N, van de Lagemaat J, Frank A J 2003 *J. Phys. Chem. B* **107** 7759
2. Kumara G R A, Konno A, Shiratsuchi K, Tsukahara J, Tennakone K 2002 *Chem. Mater.* **14** 954
3. Hara K, Kurashige M, Ito S, Shinpo A, Suga S, Sayama K, Arakawa H 2003 *Chem. Commun.* 252
4. Ferrere S, Gregg B A 2001 *J. Phys. Chem. B* **105** 7602
5. Chen S G, Chappel S, Diamant Y, Zaban A 2001 *Chem. Mater.* **13** 4629
6. Campbell W M, Burrell A K, Officer D L, Jolley K W 2004 *Coord. Chem. Rev.* **248** 1363
7. Nazeeruddin M K, Humphry-Baker R, Officer D L, Campbell W M, Burrell A K, Graetzel M 2004 *Langmuir* **20** 6514
8. Reddy P Y, Giribabu L, Lyness Ch, Snaith H J, Vijaykumar Ch, Chandrasekharan M, Lakshmi Kantam M, Yum J H, Kalyanasundaram K, Graetzel M, Nazeeruddin M K 2007 *Angew. Chem., Int. Ed.* **46** 373
9. Kuang D, Uchida S, Humphry-Baker R, Zakeeruddin S M, Graetzel M 2007 *Angew. Chem. Int. Ed.* **46** 1949
10. Tatay S, Haque S A, O'Regan B, Durrant J R, Verhees W J H, Kroon J M, Vidal-Ferran A, Gavina P, Palomares E 2007 *J. Mater. Chem.* **17** 3037
11. Giribabu L, Vijaykumar Ch, Reddy P Y, Yum J H, Graetzel M, Nazeeruddin M K 2009 *J. Chem. Sci.* **121** 75
12. Nazeeruddin M K, Angelis F D, Fantacci S, Selloni A, Viscardi G, Liska P, Ito S, Takeru B, Gratzel M 2005 *J. Am. Chem. Soc.* **127** 16835
13. Nazeeruddin M K, Pechev P, Renouard T, Zakeeruddin S M, Humphry-Baker R, Comte P, Liska P, Cevey L, Costa E, Shklover V, Spiccia L, Deacon G B, Bignozzi C A, Gratzel M 2001 *J. Am. Chem. Soc.* **123** 1613
14. Graetzel M 2005 *Inorg. Chem.* **44** 6841
15. Jiang K J, Masaki N, Xia J B, Noda S, Yanagida S 2006 *Chem. Commun.* **42** 2460
16. Chen C Y, Wu S J, Li J Y, Wu C G, Chen J G, Ho K C 2007 *Adv. Mater.* **19** 3888
17. Hum J, Jung I, Nazeeruddin M K, Gratzel M 2009 *Energy Environ. Sci.* **2** 100
18. Wang P, Zakeeruddin S M, Moser J E, Nazeeruddin M K, Sekiguchi T, Gratzel M 2003 *Nat. Mater.* **2** 402
19. Wang P, Klein C, Humphry-Baker R, Zakeeruddin S M, Graetzel M 2005 *J. Am. Chem. Soc.* **127** 808
20. Kuang D, Klein C, Ito S, Moser J-E, Baker R H, Zakeeruddin S M, Gratzel M 2007 *Adv. Funct. Mater.* **17** 154
21. Kay A, Gratzel M 1996 *Sol. Energy Mater. Sol. Cells* **44** 99
22. Saito Y, Kitamura T, Wada Y, Yanagida S 2002 *Chem. Lett.* **31** 1060
23. Suzuki K, Yamaguchi M, Kumagai M, Yanagida S 2003 *Chem. Lett.* **32** 28
24. Oskam G, Bergeron B V, Meyer G J, Searson P C 2001 *J. Phys. Chem. B* **105** 6867
25. Nusbaumer H, Moser J -E, Zakeeruddin S M, Nazeeruddin M K, Graetzel M 2001 *J. Phys. Chem. B* **105** 10461
26. Sapp S A, Elliott C M, Contado C, Caramori S, Bignozzi C A 2002 *J. Am. Chem. Soc.* **124** 11215
27. O'Regan B, Gratzel M 1991 *Nature* **353** 737
28. Nazeeruddin M K, Kay A, Rodicio I, Humphry-Baker R, Mueller E, Liska P, Vlachopoulos N, Graetzel M 1993 *J. Am. Chem. Soc.* **115** 6382

29. Hagfeldt A, Gratzel M 2000 *Acc. Chem. Res.* **33** 269
30. Gratzel M 2001 *Nature* **414** 338
31. Papageorgiou N, Athanassov Y, Armand M, Bonhôte P, Pettersson H, Azam A, Grätzel M 1996 *J. Electrochem. Soc.* **143** 3009
32. Kohle O, Gratzel M, Meyer A F, Meyer T B 1997 *Adv. Mater.* **9** 904
33. Pettersson H, Gruszecki T 2001 *Sol. Energy Mater. Sol. Cells.* **70** 203
34. Kern R, van der Burg N, Chmiel G, Ferber J, Hasenhindl G, Hinsch Sommeling P, Späth M, Uhlendorf I 2000 *Opto-Electron. Rev.* **8** 284
35. Hinsch A, Koorn J M, Kern R, Uhlendorf I, Holzbock J, Meyer A, Ferber J 2001 *Prog. Photovoltaics* **9** 425
36. Pettersson H, Gruszecki T, Johansson L -H, Johander P 2003 *Sol. Energy Mater. Sol. Cells* **77** 405
37. Ajayaghosh A, Carol P, Sreejith S 2005 *J. Am. Chem. Soc.* **127** 14962
38. Sreejith S, Divya K P, Ajayaghosh A 2008 *Chem. Commun.* **44** 2903
39. Divya K P, Sreejith S, Balakrishna B, Jayamurthy P, Aneesa P, Ajayaghosh A 2010 *Chem. Commun.* **46** 6069
40. Giribabu L, Vijay Kumar Ch, Srinivasa Rao Ch, Gopal Reddy V, Yella Reddy P, Chandrasekharan M, Soujanya Y 2009 *Energy Environ. Sci.* **2** 770
41. Chandrasekharan M, Srinivasarao Ch, Suresh T, Anil Reddy M, Raghavender M, Rajkumar G, Srinivasu M, Yella Reddy P 2011 *J. Chem. Sci.* **123** 37
42. Chandrasekharan M, Rajkumar G, Srinivasa Rao Ch, Suresh T, Reddy P Y 2011 *Syn. Met.* **161** 1469–1476
43. Chandrasekharan M, Rajkumar G, Srinivasa Rao Ch, Suresh T, Soujanya Y, Reddy P Y 2011 *Adv. Optoelectronics* (accepted). doi:[10.1155/2011/432803](https://doi.org/10.1155/2011/432803)
44. Chen R, Yang X, Tian H, Wang X, Hagfeldt A, Sun L 2007 *Chem. Mater.* **19** 4009
45. Gao F, Wang Y, Shi D, Zhang J, Wang M, Jing X, Humphry-Baker R, Wang P, Zakeeruddin S M, Gratzel M 2008 *J. Am. Chem. Soc.* **130** 10720
46. Miyaura N, Suzuki A 1995 *Chem. Rev.* **95** 2457
47. Li Z H, Wong M- S, Tao Y, Lu J 2005 *Chem. Eur. J.* **11** 3285
48. Bennett M A, Huang T N, Matheson T W, Smith A K 1982 *Inorganic Syntheses* **21** 74
49. Gillaiseau I, Gauthier Odobel F, Alebbi M, Argazzi R, Costa E, Alberto Bignozzi C, Qu P, Meyer G J 2001 *Inorg. Chem.* **40** 6073
50. Yu Q, Liu S, Zhang M, Cai N, Wang Y, Wang P 2009 *J. Phys. Chem. C* **113** 14559
51. Hay P J, Wadt W R 1985 *J. Chem. Phys.* **82** 299
52. Kopidakis N, Neale N R, Frank A J 2006 *J. Phys. Chem. B* **110** 12485